Archives of Biochemistry and Biophysics 539 (2013) 81–86

Contents lists available at ScienceDirect

Archives of Biochemistry and Biophysics

journal homepage: www.elsevier.com/locate/yabbi

Mechanism of cysteine oxidation by peroxynitrite: An integrated experimental and theoretical study

Ari Zeida [a], Mariano C. González Lebrero [b], Rafael Radi [c], Madia Trujillo [c,*], Darío A. Estrin [a,*]

[a] Departamento de Química Inorgánica, Analítica y Química-Física and INQUIMAE-CONICET, Facultad de Ciencias Exactas y Naturales, Universidad de Buenos Aires, Buenos Aires, Argentina
[b] IQUIFIB-Dpto. Química Biológica, Facultad de Farmacia y Bioquímica, Universidad de Buenos Aires, Buenos Aires, Argentina
[c] Departamento de Bioquímica and Center for Free Radical and Biomedical Research, Facultad de Medicina, Universidad de la República, Montevideo, Uruguay

ARTICLE INFO

Article history:
Received 19 June 2013
and in revised form 13 August 2013
Available online 4 September 2013

Keywords:
Thiols
Cysteine
Peroxynitrite
Oxidation
S_N2
Redox homeostasis

ABSTRACT

Since peroxynitrite was identified as a pathophysiological agent it has been implicated in a great variety of cellular processes. Particularly, peroxynitrite mediated oxidation of cellular thiol-containing compounds such as Cys residues, is a key event which has been extensively studied. Although great advances have been accomplished, the reaction is not completely understood at the atomic level. Aiming to shed light on this subject, we present an integrated kinetic and theoretical study of the oxidation of free Cys by peroxynitrite. We determined pH-independent thermodynamic activation parameters, namely those corresponding to the reaction between the reactive species: Cys thiolate and peroxynitrous acid. We found a pH-independent activation energy of 8.2 ± 0.6 kcal/mol. Simulations were performed using state of the art hybrid quantum–classical (QM–MM) molecular dynamics simulations. Our results are consistent with a S_N2 mechanism, with Cys sulfenic acid and nitrite anion as products. The activation barrier is mostly due to the alignment of sulfur's thiolate atom with the oxygen atoms of the peroxide, along with the concomitant charge reorganization and important changes in the solvation profile. This work provides an atomic detailed description of the reaction mechanism and a framework to understand the environment effects on peroxynitrite reactivity with protein thiols.

Introduction

Oxidation of free Cys,[1] GSH or Cys residues in proteins, is a key event implicated in a great variety of cellular processes such as antioxidant responses, signal transduction, regulation of the activity of enzymes, protein channels and/or transcription factors [1–6]. Peroxynitrite (as the sum of peroxynitrite anion (−1) and peroxinitrous acid)[2] is formed in the cell by the fast reaction between superoxide anion ($O_2^{\cdot-}$) and nitric oxide ($^{\cdot}NO$) radicals, with a second order rate constant of about 10^9–10^{10} M^{-1} s^{-1} [7,8]. ONOOH has a *pKa* between 6.5–6.8 [7–9], and decays producing hydroxyl ($^{\cdot}OH$) and nitrogen dioxide ($^{\cdot}NO2$) radicals in ~30% yields ($k = 0.9\ s^{-1}$, pH 7.4, 37 °C) [5,8,10]. Both ONOOH and $ONOO^-$ are strong oxidants which react with different cell molecular components and since the first proposal as a pathophysiological agent [11–14], these species have been implicated in a numerous biologically relevant processes associated with protein function modification and cellular signaling among others (for comprehensive reviews see Ref. [15–16]). Particularly, the two-electron oxidation of free Cys by peroxynitrite has been studied from a kinetic approach [14,17,18]. The process is actually carried out by the thiolate form of Cys ($CysS^-$) and ONOOH [9,18], through the reaction:

$$CysS^- + ONOOH \rightarrow RSOH + NO_2^- \quad (1)$$

The second order rate constant has been reported as 5–6 × 10^3 M^{-1} s^{-1} (37 °C), with an activation energy of about 9.7 kcal/mol (pH 7.5) [14,17]. The reaction has been proved to be strongly pH-dependent [14].

Although the reactivity of low molecular weight thiols and some protein Cys residues like human serum albumin can be related with thiol acidity constants, some proteins like peroxiredoxins or glyceraldehydes 3-phosphate dehydrogenase show a much higher reactivity than the expected just from inspecting thiol's *pKa*, [19–22] indicating that besides this factor, the environment surrounding thiol groups is critical to comprehend this phenomenon and it is important to get a molecular viewpoint of this reaction.

* Corresponding author. Address: Ciudad Universitaria, Pab. 2, C1428EHA, Buenos Aires, Argentina. Fax: +54 11 45763341 (D.A. Estrin). Address: Av. Gral Flores 2125, CP 11800, Montevideo, Uruguay. Fax: +598 29249563 (M. Trujillo).
E-mail addresses: madiat@fmed.edu.uy (M. Trujillo), dario@qi.fcen.uba.ar (D.A. Estrin).

[1] *Abbreviations used:* Cys, L-cysteine; $CysS^-$, cysteinate; CysSOH, cysteine sulfenic acid; GSH, glutathione; DFT, density functional theory; QM, quantum mechanics; MM, molecular mechanics; MD, molecular dynamics; dzvp, double zeta valence with polarization; IRC, intrinsic reaction coordinate.

[2] The IUPAC recommended names for peroxynitrite anion and peroxynitrous acid are, oxoperoxonitrate (1-) and hydrogen oxoperoxonitrate, respectively.

0003-9861/$ - see front matter © 2013 Elsevier Inc. All rights reserved.
http://dx.doi.org/10.1016/j.abb.2013.08.016

In order to contribute to this understanding, we present here an integrated kinetic and theoretical approach of the oxidation of cysteine presented in Eq. (1). pH-independent thermodynamic activation parameters were determined from kinetics experiments. The reaction mechanism and system properties were evaluated on the basis of hybrid QM–MM MD simulations combined with an umbrella sampling scheme, which allow us to achieve free energies and the evolution of the electronic properties along the reaction coordinate, within a realistic representation of the aqueous environment [23]. This work represents the first theoretical study of this important reaction. Our results underline the pH dependency of the process and the solvent significance, assisting in the orientation of ONOOH and allowing the charge reorganization to take place. The data presented herein set the basis for further integrated studies on the mechanism of thiol oxidation in different protein environments.

Materials and methods

Chemicals

L-Cysteine, diethylenetriaminepentaacetic acid (dtpa), 5,5′-dithiobis(2-nitrobenzoate) (DTNB), and sodium phosphate salts were purchased from Sigma–Aldrich. Peroxynitrite was synthesized from H_2O_2 and nitrous acid as described previously [11,14]. Stock solutions of peroxynitrite were treated with granular manganese dioxide to eliminate remaining H_2O_2. Nitrite contamination was typically < 30% of peroxynitrite concentration [24].

Kinetics experiments

All experiments were performed in 100 mM sodium phosphate buffer containing 0.1 mM dtpa. Differential mixing of mono- and di-basic phosphate buffers were performed in order to achieve different pHs. Ionic strength was kept constant (0.15 mM) with the addition of NaCl.

Peroxynitrite concentration was determined at alkaline pH at 302 nm (ε_{302} = 1670 $M^{-1}cm^{-1}$) and was equal to 0.1 mM in the mix. Thiol content of Cys solutions was measured by Ellman's assay (ε_{412} = 14150 $M^{-1}cm^{-1}$) [25] and was varied between 6.0 and 13.0 mM in the final mix.

Kinetics of peroxynitrite decomposition was followed by absorbance spectroscopy (λ = 302 nm) in an Applied Photophysics SX-20 stopped-flow spectrofluorimeter (mixing time of $\leqslant$ 1.2 ms). Outlets pH measurements were always done at bath temperature (namely 10, 25, 37 and 50 °C). Each observed rate constant, which correspond to pH-dependent first order rate constants (k_{1app}) of peroxynitrite decay, was determined by fitting at least 5 data sets to single exponential functions. Firstly, ONOOH auto-decay pH-independent rate constants were determined for each temperature, fitting k_{1app} constants versus pH:

$$k_{1app} = k_1\left(\frac{10^{-pH}}{10^{-pKa_{ONOOH}} + 10^{-pH}}\right) \quad (2)$$

Then, pH-dependent second order rate constants (k_{2app}) for the reaction between cysteine and peroxynitrite were determined, following peroxynitrite decay in the presence of excess Cys under different conditions of pHs and temperatures. Experimental data were fitted to single exponentials, from which k_{obs} values were obtained.

Since in this case $k_{obs} = k_{1app} + k_{2app}$ x [Cys], k_{2app} were determined by subtracting the corresponding auto-decay rate at exactly the same pH and dividing by Cys concentration (two different Cys concentrations were usually used at each pH and temperature, with identical results). This method was preferred over rate constant determinations at multiple Cys concentrations at a single pH for each pH and temperature, to rigorously control pH values when using acidic stock solutions of Cys and to avoid Cys stock oxidation during the experiment that could occur if Cys stock solutions were neutralized. For selected pHs and temperatures, both methodologies were used yielding the same results.

As a result, pH-independent second order rate constants were calculated from the fitting of the plot of k_{2app}versus pH:

$$k_{2app} = k_2\left(\frac{10^{-pKa_{Cys}}}{10^{-pKa_{Cys}} + 10^{-pH}}\right)\left(\frac{10^{-pH}}{10^{-pKa_{ONOOH}} + 10^{-pH}}\right) \quad (3)$$

Classical Arrhenius and Eyring's analysis were then performed over the data obtained as explained above.

Computer simulations

Initial survey of the system

In order to obtain information about the energy surface and the mechanism of the reaction under investigation, and to carry out a methodology evaluation, we performed several electronic structure calculations using *Gaussian 03* [26]. The structures of reactants ($CysS^-$ and ONOOH) and reactant complex (RC) ($CysS^-$/ONOOH), products complex (PC) (CysSOH/NO_2^-) and transition state (TS) were optimized both in vacuo and in the presence up to 4 water molecules at different levels of theory: *HF*, *PBE*, *B3LYP*, *MP2*, employing a double-zeta plus polarization (*dzvp*) Gaussian basis set [27]. Frequency calculations were performed in all cases. Aiming to investigate if one or more water molecules could be involved in the reaction mechanism, we also performed IRC calculations at the *PBE/dzvp* level of theory including one and four water molecules in the QM system.

ONOOH *B3LYP* calculation was used to get classical parameters of this moiety [28], necessaries to perform the classical MD simulations which are required to equilibrate the systems, as described below.

QM–MM molecular dynamics simulations

The actual QM–MM simulations were carried out using the code and parameters described in Ref. [23] (for details on the QM–MM scheme see Refs. [29–30]). The system consisted in the quantum solute ($CysS^-$ + ONOOH) embedded in a box containing 3247 classical TIP4P water molecules. For the QM region, computations were performed at the generalized gradient approximation (GGA) level, using the *PBE* combination of exchange and correlation functionals, with a *dzvp* basis set for the expansion of the one-electron orbitals [27]. All the QM–MM MD simulations were run for at least 5 ps and employed the Verlet algorithm to integrate Newton's equations with a time step of 0.2 fs. Initial configurations were generated from preliminary 100 ps classical equilibration runs in which the solute was treated classically as a rigid moiety, followed by a QM–MM MD where the solute was treated at the *AM1* semi-empirical level, as implemented in Amber [31].

To explore reaction's free energy and mechanism, we employed an umbrella sampling scheme, choosing as reaction coordinate the difference between the O_1–O_2 and the S–O_1 distances (see Fig. 2), which was sampled from −1.8 to 1.0 Å, divided in 29 simulations windows.

All dynamics visualizations and molecular drawings, were performed with VMD 1.8.6. [32].

Results and discussion

pH-independent reaction parameters

The kinetics of the oxidation mediated by peroxynitrite of low molecular weight thiols like Cys and GSH [14,17] or Cys residues

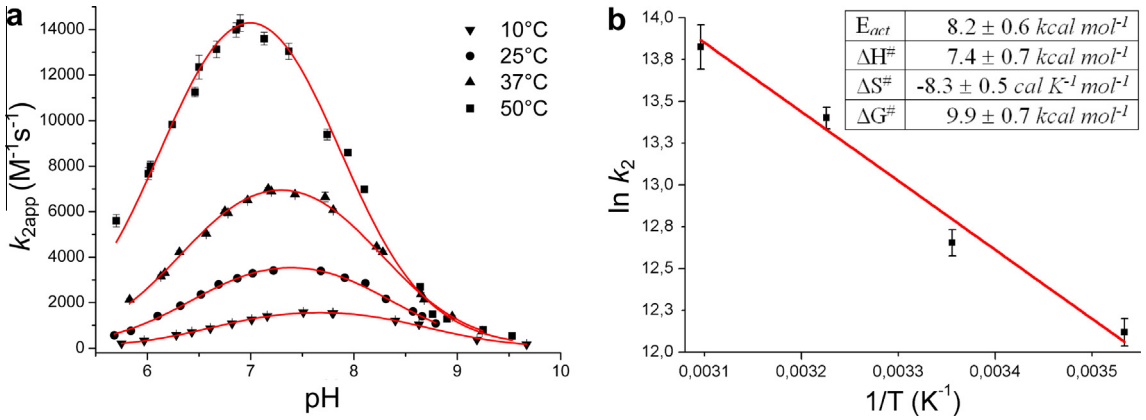

Fig. 1. Kinetics of the oxidation of Cys by peroxynitrite. (a) "Bell-shaped" plots of the dependence of k_{2app} (M^{-1} s^{-1}) as a function of pH, at T = 10, 25, 37 and 50 °C. k_{2app} refers to apparent, pH-dependent second order rate constants. (b) Consequent Arrhenius plot. Values of thermodynamic pH-independent activation parameters derived from this plot and subsequent Eyring's analysis are also shown. $\Delta G^{\#}$ is calculated at 37 °C.

in proteins like human serum albumin [33] and a variety of peroxiredoxins [22–34] has been studied since peroxynitrite was proposed as a pathophysiological agent [11–14]. As described before [9,18], the two-electron oxidation process occurs between the thiolate anion and ONOOH, therefore the fraction of the reactive species depend strongly on the medium pH. Fig. 1 shows the Arrhenius plot of the reaction between $CysS^-$ and ONOOH. Note that the analysis is performed considering pH-independent rate constants, determined at 10, 25, 37 and 50 °C (see Materials and Methods).

Arrhenius analysis determines a pH-independent activation energy of 8.2 ± 0.6 kcal/mol, to some extent lower than the one reported by Koppenol et al., at pH 7.5, which was 9.7 kcal/mol [17]. This difference could be due to the fact that in the range of explored temperatures and pHs, pKa_{Cys} varies significantly more than pKa_{ONOOH} (see Table S1 of supplementary information), decreasing as temperature increases and so allowing a higher ratio thiolate/thiol [35]. From the data shown in Table S1 and using Van't Hoff equation, an standard enthalpy of Cys thiol ionization of 7.8 kcal/mol was estimated, very similar to values previously reported [35]. On the contrary, ionization of ONOOH fraction was less affected by temperature, in agreement with a lower standard enthalpy of ionization of ONOOH, which has been reported as 4.1 ± 1.6 kcal/mol [36]. Additionally, it should be noted that we systematically repeated the determination of k_2 at 37 °C and pH 7.4, obtaining a value of 6,635 ± 335 M^{-1} s^{-1} (see Fig. S1 of supplementary information), somehow higher than the reported before, probably owing to slightly different experimental conditions [14].

Subsequent Eyring's analysis gives a $\Delta H^{\#}$ = 7.4 ± 0.7 kcal/mol and $\Delta S^{\#}$ = −8.3 ± 0.5 cal/K.mol, therefore the pH-independent activation Gibbs free energy results in 9.9 ± 0.7 kcal/mol (calculated at 37 °C). As will be shown in the next section, the negative value of $\Delta S^{\#}$ is consistent with a TS much more rigid structure than the reactants in the ground state, in which degrees of freedom of translation and rotation are "frozen". Moreover, at this temperature the $-T\Delta S^{\#}$ factor constitutes a quarter of the total $\Delta G^{\#}$, so it is essential to account to this contribution in the comparison of this aqueous reaction with enzymes environments, and their catalytic capabilities to stabilize the TS and therefore decrease $\Delta G^{\#}$ [37].

Although $ONOO^-$ and ONOOH alone, have been the subject of several theoretical studies (for some examples see Refs. [38–41]), this is the first attempt to tackle this important reaction by means of a quantum mechanical approximation. Using the QM–MM scheme as described above, we performed umbrella sampling calculations in order to obtain the free energy profile of the oxidation of $CysS^-$ by ONOOH, which is depicted in Fig. 2,a.

The analysis exhibits a clearly exergonic process with a ΔG_{rxn} ≈ −46 kcal/mol, in agreement with purely quantum mechanics calculations (see Table S2 of supplementary information). The profile also shows an early TS associated with a free energy activation barrier of about 5 kcal/mol, somewhat smaller than the experimentally determined. The study of the electronic structure of peroxynitrite and its derivates, it is rather subtle; even correlated methods as *MP2* fails to describe accurately certain properties of these systems [42]. Particularlly, *DFT* methods at the GGA level provides underestimated barriers related to the stability of the weakly bound O−O peroxy-bond of these kind of systems, and much better results can be found calculating the barriers using *postHF* or hybrid *DFT* approximations over *DFT* structures [30,39]. In order to test that the sampled reaction pathway in our QM–MM simulations is not dissimilar from what is suggested using different methodologies, we analyze the geometries of the RC, TS and PC obtained for several methods and density functionals, corroborating a great equivalence between them (see Table S3 supplementary information). Therefore, we calculate $\Delta G^{\#}$ and ΔG_{rxn} as $\Delta G_{QM/MM} - \Delta G^{solute}_{PBE} + \Delta G^{solute}_{MP2/B3LYP}$, in order to improve the *PBE* functional energy prediction (Fig. 2b). The *MP2* corrected result ($\Delta G^{\#}$ = 8.4 kcal/mol) is in very good agreement with the experimental measurement.

Microscopic basis of the reaction mechanism

Our QM–MM scheme allows us to get a microscopic insight into the reaction mechanism, as well as the evolution of the different system properties (see the 3D animation available in Supporting Information for illustration).

Fig. 3 shows the relevant distances evolution along the reaction coordinate. At the reactants, the interaction between $CysS^-$ and ONOOH is due to the hydrogen bond between S and O1, and the system samples a lot of different conformations in which this interaction is conserved. In the early TS, the arrangement looses degrees of freedom and it can be observed an alignment of S, O1 and O2 atoms, along with a concomitant shortening of the O2−N bond. Previous studies on the oxidation of thiols by hydrogen peroxide, have demonstrated the occurrence of a proton transfer after yielding the TS, from the derived sulfenic acid to the OH^- to give a water molecule as a product [23,43]. It should be noted that we do not observe the mentioned transference in the reaction with peroxynitrite studied herein, which is then perfectly consistent with a sub-

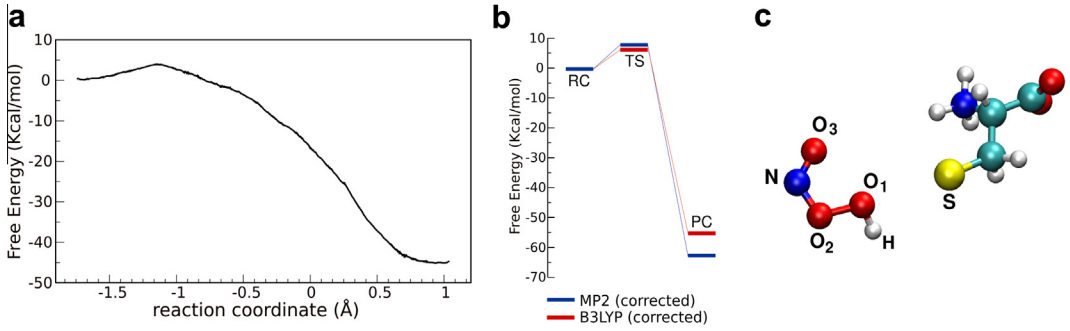

Fig. 2. (a) Free energy profile obtained by the QM–MM umbrella sampling. Free energy (kcal/mol) is plotted versus reaction coordinate (Å), which was set as the difference between the O_1-O_2 and the $S-O_1$ distances. (b) Corrected free energies calculated as $\Delta G_{QM/MM} - \Delta G_{PBE}^{solute} + \Delta G_{MP2/B3LYP}^{solute}$. (c) Illustrative picture of the QM system with the atoms names as referred in the text.

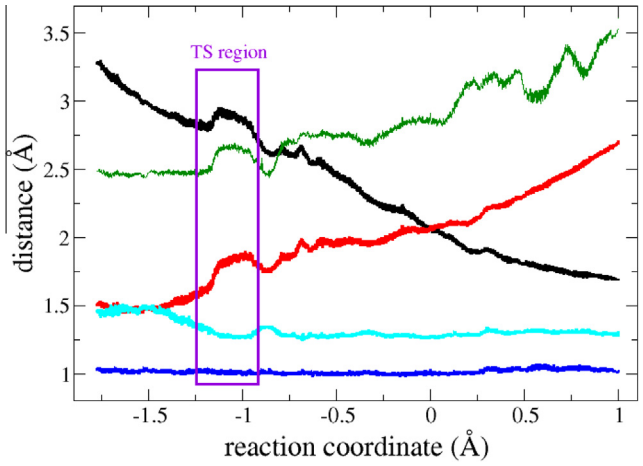

Fig. 3. Bond length evolution during the reaction. The S–O1 (black), O1–O2(red), O1–H (blue), O1–N (green) and O2–N (light blue) distances (Å) as a function of the reaction coordinate (Å) are depicted. The TS region (as determined in Fig. 1) is indicated by a dark violet box. (For interpretation of the references to color in this figure legend, the reader is referred to the web version of this article.)

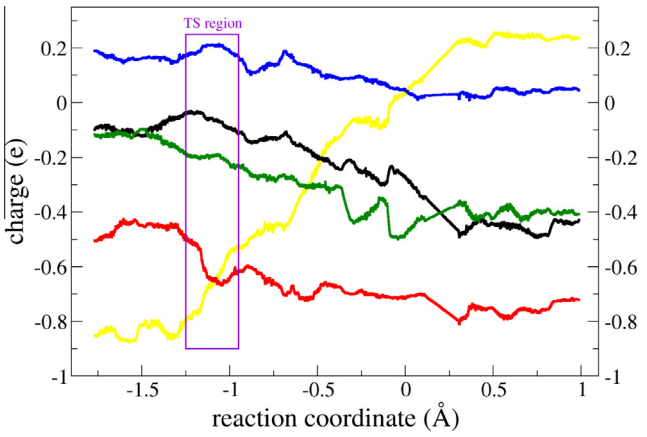

Fig. 4. Charge evolution during the reaction. Mulliken charges (e) of S atom (yellow line), O1 atom (red line), O2 atom (black line), N atom (blue line) and O3 atom (green line) are plotted versus the reaction coordinate (Å). The TS region (as determined in Fig. 1) is indicated by a dark violet box. (For interpretation of the references to color in this figure legend, the reader is referred to the web version of this article.)

stitution like mechanism. Furthermore, the O1–H distance remains close to 1 Å during the whole path, concluding in the protonated CysSOH and NO_2^- as the products of the process.

Charges distribution and rearrangement is observed in Fig. 4. The initial attack of the S atom to O1 atom take place between two negatively charged centers, however it is a nucleophilic attack, since O1 atom acts as an electrophile, turning into a more negative charged atom along the reaction. Even though the final dissociation of the peroxide O1–O2 bond is homolytic, the reorganization of oxygen charges is not entirely symmetric. During the first stages of the reaction, the charge that it is lost by the S atom is gained mostly by O1. Only after the TS, the system negative charge gets distributed on the NO_2^- moiety. As expected, O1 atom in the CysSOH product has a strong negative charge, and the −1 charge on the nitrite anion is equally distributed between O2 and O3. These data perfectly agree with the experimentally determined Brønsted correlation between the pH-independent second order rate constants of peroxynitrite reduction by thiolates, which shows a nucleophilicity constant of ∼0.4 [19], indicating a partial electron pair donation from the nucleophililic thiolate at the transition state.

There have been preceding efforts into understanding the influence of the solvent in these type of molecular systems [40,42–45]. The QM–MM methodology implemented in this work, allows to account to the environment impact in an accurate way [29]. As can be seen in Fig. 5, the changes in the solvation profiles are intimately associated with the electronic distribution. While the S atom looses its hydrophilicity during the course of the reaction, O1 atom is much better solvated already at the TS, and both O2 and O3 improve considerably their solvation structures in the products. A global analysis enables to observe how the products improve the interaction with the aqueous environment compared with reactants.

In summary, the reaction occurs via the nucleophilic attack of the thiolate's S atom on the O1 atom of the peroxide, with a nitrite anion (NO_2^-) as the leaving group, in a classical S_N2 nucleophilic substitution. The free energy barrier is mostly due to the appreciable electronic reorganization together with the changes in the solvation structure, associated with the alignment of S, O1 and O2 atoms, the shortening of S–O1 and O2–N bonds and the elongation of O1–O2 union.

Beyond free Cys or GSH capacity to reduce peroxynitrite, a great variety of Cys protein residues have been tested in this sense. Different effects can be observed: thiols in some proteins like that of the single free Cys in human serum albumin [33] and *Trypanosoma brucei* tryparedoxin [46] exhibits comparable second order rate constants than those of low molecular weight thiols, others like glyceraldehyde 3-phosphate dehydrogenase or creatine quinase show a ∼100-fold acceleration on the rates [21,47]. Taking into

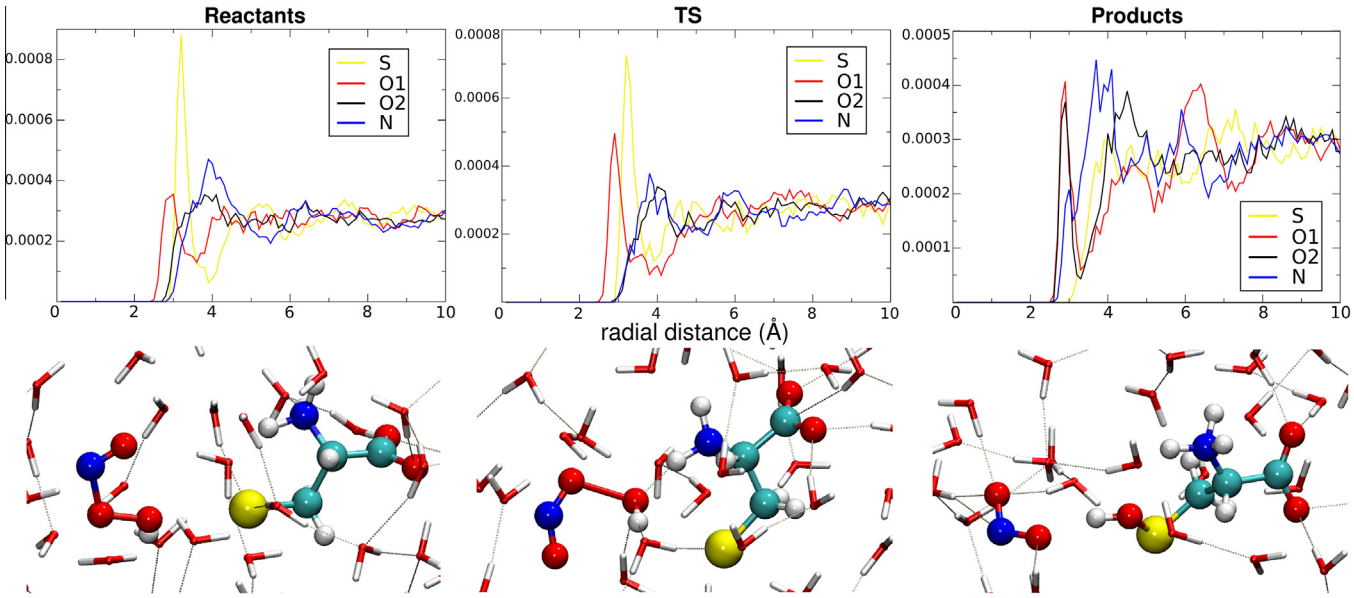

Fig. 5. Solvation structure during the reaction. Up: radial correlations functions of S, O1, O2 and N with water oxygen atoms from the reactants (left panel), TS (middle panel) and products (right panel). Down: representative snapshots of the solvation structure of the reactants (left panel), TS (middle panel) and products (right panel).

account enzyme physiological concentrations and kinetics, peroxiredoxins becomes the most efficient peroxynitrite scavengers, displaying pH-independent rate constants between 10^2–10^4 times faster than free Cys or other low molecular weight thiols [22]. Recently, structural analyses of peroxiredoxins active site, proposed a series of microenviromental factors that could lead to TS stabilization [48]. The results presented here highlights the significance for the protein environment that surrounds these reactive Cys residues, to assist in the correct orientation of the peroxide, the alignment of the S atom with the peroxide oxygen atoms in the TS [48–50], allowing the charge reorganization to take place.

Conclusions

We present here an integrated experimental and theoretical study of the oxidation of Cys by peroxynitrite, which allow us to get kinetic, thermodynamic and microscopic dynamical information of this reaction in aqueous environment. Rate constants and activation energies obtained are in good agreement with previous reported experimental data [14,17,22] and small differences are discussed. To the best of our knowledge, this is the first theoretical approximation to this particular process.

We found the pH-independent activation energy to be slightly smaller than the reported one at pH 7.5 [17]. Additionally, the reaction shows a noteworthy negative $\Delta S^{\#}$, which significantly contributes to $\Delta G^{\#}$ ($-T\Delta S^{\#}$ ~25%), highlighting this parameter importance in comparing the same process embedded in different microenvironments. Although the calculations presented herein suggests that no water molecules participates covalently in the oxidation, simulations confirms the solvent significance and great changes in the solvation structure can be observed already in the TS, underlining the key role of the environment in modulating thiol reactivity.

In this context, it is essential to achieve atomistic detailed information about the mechanism of thiol containing compounds oxidation with peroxides. This study creates the foundation to experimental and theoretical studies that are underway in our laboratories, in order to contribute on the mechanisms of fast reacting thiols oxidation and its reactivity modulation in proteins.

Funding support

This work was partially supported by the University of Buenos Aires, CONICET and Centro de Biología Estructural Mercosur (CEBEM). The calculations have been performed in FCEN CECAR and MINCyT Cristina computer centers. MT and RR acknowledge the financial support of the Agencia Nacional de Investigación e Innovación (FCE_2011_1_5706, ANII, Uruguay), Comisión Sectorial de Investigación Científica (CSIC), Universidad de la República and the National Institutes of Health (RO1 AI095173).

Appendix A. Supplementary data

Supplementary data associated with this article can be found, in the online version, at http://dx.doi.org/10.1016/j.abb.2013.08.016.

References

[1] L.B. Poole, K.J. Nelson, Curr. Opin. Chem. Biol. 12 (2008) 18–24.
[2] A. Bindoli, J.M. Fukuto, H.J. Forman, Antioxid. Redox Signal. 10 (2008) 1549–1564.
[3] L.B. Poole, P.A. Karplus, A. Claiborne, Annu. Rev. Pharmacol. Toxicol. 44 (2004) 325–347.
[4] A. Claiborne, J.I. Yeh, T.C. Mallett, J. Luba, E.J. Crane, D. Parsonage, Biochemistry 38 (1999) 15407–15416.
[5] J.B. Schulz, J. Lindenau, J. Seyfried, J. Dichgans, Eur. J. Biochem. 267 (2000) 4904–4911.
[6] Y.M. Go, D.P. Jones, Free Radic. Biol. Med. 4 (2011) 495–509.
[7] S. Goldstein, G. Czapski, Free Radic. Biol. Med. 19 (1995) 505–510.
[8] R. Kissner, T. Nauser, P. Bugnon, P.G. Lye, W.H. Koppenol, Chem. Res. Toxicol. 10 (1997) 1285–1292.
[9] W.A. Pryor, G.L. Squadrito, Am. J. Physiol. 268 (1995) 699–722.
[10] O.V. Gerasimov, S.V. Lymar, Inorg. Chem. 38 (1999) 4317–4321.
[11] J.S. Beckman, T.W. Beckman, J. Chen, P.A. Marshall, B.A. Freeman, Proc. Natl. Acad. Sci. USA 87 (1990) 1620–1624.
[12] H. Ischiropoulos, L. Zhu, J. Chen, M. Tsai, J.C. Martin, C.D. Smith, J.S. Beckman, Arch. Biochem. Biophys. 298 (1992) 431–437.
[13] R. Radi, J.S. Beckman, K.M. Bush, B.A. Freeman, Arch. Biochem. Biophys. 288 (1991) 481–487.
[14] R. Radi, J.S. Beckman, K.M. Bush, B.A. Freeman, J. Biol. Chem. 266 (1991) 4244–4250.
[15] G. Ferrer-Sueta, R. Radi, ACS Chem. Biol. 4 (2009) 161–177.
[16] P. Pacher, J.S. Beckman, L. Liaudet, Physiol. Rev. 87 (2007) 315–424.
[17] W.H. Koppenol, J.J. Moreno, W.A. Pryor, H. Ischiropoulos, J.S. Beckman, Chem. Res. Toxicol. 5 (1992) 834–842.
[18] M. Trujillo, R. Radi, Arch. Biochem. Biophys. 397 (2002) 91–98.

[19] M. Trujillo, A. Clippe, B. Manta, G. Ferrer-Sueta, A. Smeets, J.P. Declercq, B. Knoops, R. Radi, Arch. Biochem. Biophys. 467 (2007) 95–106.
[20] M. Dubuisson, D. Vander Stricht, A. Clippe, F. Etienne, T. Nauser, R. Kissner, W.H. Koppenol, J.F. Rees, B. Knoops, FEBS Lett. 571 (2004) 161–165.
[21] J.M. Souza, R. Radi, Arch. Biochem. Biophys. 360 (1998) 187–194.
[22] M. Trujillo, B. Alvarez, J.M. Souza, N. Romero, L. Castro, L. Thomson, R. Radi, in: L. Ignarro (Ed.), Nitric Oxide Biology and Pathobiology, Academic Press, California, 2010, pp. 61–402.
[23] A. Zeida, R. Babbush, M.C. González Lebrero, M. Trujillo, R. Rafael Radi, D.A. Estrin, Chem. Res. Toxicol. 25 (2012) 741–746.
[24] B. Alvarez, V. Demicheli, R. Durán, M. Trujillo, C. Cerveñansky, B.A. Freeman, R. Radi, Free Radic. Biol. Med. 37 (2004) 813–822.
[25] G.L. Ellman, Arch. Biochem. Biophys. 82 (1959) 70–77.
[26] Gaussian 03, Gaussian, Inc.: Wallingford, CT, 2004.
[27] N. Godbout, D.R. Salahub, J. Andzelm, E. Wimmer, Can. J. Chem. 70 (1992) 560–571.
[28] C.I. Bayly, P. Cieplak, W.D. Cornell, P.A. Kollman, A well-behaved electrostatic potential based method using charge restraints for determining atom-centered charges: the RESP model, J. Phys. Chem. 97 (1993) 10269–10280.
[29] M.C. González Lebrero, D.E. Bikiel, M.D. Elola, D.A. Estrin, A.E. Roitberg, J. Chem. Phys. 117 (2002) 2718–2725.
[30] M.C. González Lebrero, D.A. Estrin, J. Chem. Theory Comput. 3 (2007) 1405–1411.
[31] D.A. Case, AMBER 11, University of California, San Francisco, 2010.
[32] W. Humphrey, A. Dalke, K. Schulten, J. Mol. Graphics 14 (1996) 33–38.
[33] B. Alvarez, G. Ferrer-Sueta, B.A. Freeman, R. Radi, J. Biol. Chem. 274 (1999) 842–848.
[34] R. Bryk, P. Griffin, C. Nathan, Nature 407 (2000) 211–215.
[35] M.Y. Torchinsky, in: M.Y. Torchinsky (Ed.), Sulfur in Proteins, Pergamon Press, New York, 1981, pp. 3–18.
[36] W.H. Koppenol, R. Kissner, Chem. Res. Toxicol. 2 (1998) 87–90.
[37] P.S. Low, J.L. Bada, G.N. Somero, Proc. Natl. Acad. Sci. USA 70 (1973) 430–432.
[38] B.S. Jursic, L. Klasnic, S. Pecur, W.A. Pryor, Nitric Oxide 1 (1997) 494–501.
[39] R.D. Bach, M.N. Glukhovtsev, C. Canepa, J. Am. Chem. Soc. 120 (1998) 775–783.
[40] D.A. Dixon, D. Feller, C.-G. Zhan, J.S. Francisco, J. Phys. Chem. A 106 (2002) 3191–3196.
[41] D.G. Musaev, K. Hirao, J. Phys. Chem. A 107 (2003) 1563–1573.
[42] M.C. González Lebrero, L.L. Perissinotti, D.A. Estrin, J. Phys. Chem. A 109 (2005) 9598–9604.
[43] B. Cardey, M. Enescu, ChemPhysChem 6 (2005) 1175–1180.
[44] B. Cardey, M. Enescu, J. Phys. Chem. A 111 (2007) 673–678.
[45] K. Doclo, U. Rothlisberger, J. Phys. Chem. A 104 (2000) 6464–6469.
[46] M. Trujillo, H. Budde, M.D. Piñeyro, M. Stehr, C. Robello, L. Flohé, R. Radi, J. Biol. Chem. 279 (2004) 34175–34182.
[47] E.A. Konorev, N. Hogg, B. Kalyanaraman, FEBS Lett. 427 (1998) 171–174.
[48] A. Hall, D. Parsonage, L.B. Poole, P.A. Karplus, J. Mol. Biol. 402 (2010) 194–209.
[49] P.A. Karplus, A. Hall, Structural survey of the peroxiredoxins: structures and functions, in: L. Flohe, J.R. Harris (Eds.), Peroxiredoxins Systems, Springer, New York, 2007, pp. 41–60.
[50] A. Hall, K. Nelson, L.B. Poole, P.A. Karplus, Antioxid. Redox Signal. 15 (2011) 795–815.